

Polymorphism, Structure, and Nucleation of Cholesterol.H₂O at Aqueous Interfaces and in Pathological Media: Revisited from a Computational Perspective

Margarita Shepelenko,^a Anna Hirsch,^a Neta Varsano,^b
Lia Addadi,^b Leeor Kronik,^{*a} and Leslie Leiserowitz^{*a}

^aDepartment of Molecular Chemistry and Materials Science, Weizmann Institute of Science, Rehovoth 76100, Israel

^bDepartment of Chemical and Structural Biology, Weizmann Institute of Science, Rehovot 76100, Israel

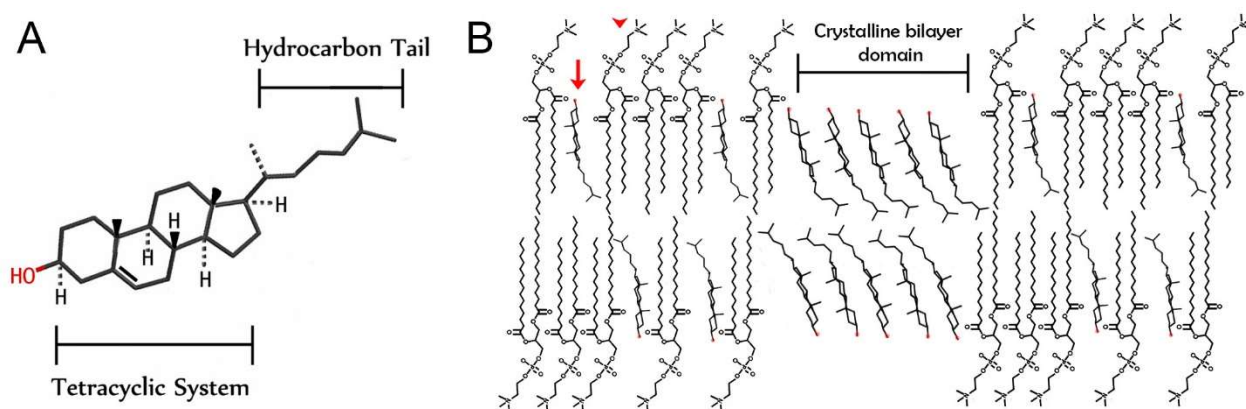
*To whom correspondence should be addressed. Email: leeor,kronik@weizmann.ac.il; Leslie.Leiserowitz@weizmann.ac.il

Abstract

We revisit the important issues of polymorphism, structure, and nucleation of cholesterol monohydrate, using first principles calculations based on dispersion-augmented density functional theory. For the lesser known monoclinic polymorph, we obtain a new, fully extended H-bonded network, comprising the sterol hydroxyl groups and water molecules in a structure akin to that of hexagonal ice. We show that the energy of the monoclinic and triclinic polymorphs is similar, strongly suggesting that kinetic and environmental effects play a significant role in determining polymorph nucleation. Furthermore, we find evidence in support of various O-H \cdots O bonding motifs, in both polymorphs, that may result in structural disorder. We then rationalize what we believe is a single-crystal to single-crystal transformation of the monoclinic form on increased interlayer growth beyond that of a single cholesterol bilayer, interleaved by a water bilayer, and show that the ice-like structure is also relevant to the related cholestanol dihydrate (2H₂O) crystal. Finally, we posit a possible role for cholesterol esters in the crystallization of cholesterol.H₂O in pathological environments, with a composite of a bilayer of cholesteryl palmitate bound epitaxially as a nucleating agent to the monoclinic form of cholesterol.H₂O.

I. Introduction

Cholesterol, the most abundant sterol in mammalian cells, is a vital component of cell membranes and is essential for cell viability.⁽¹⁾ The cholesterol molecule consists of one hydroxyl group attached to a rigid steroid tetracyclic moiety, terminating with a flexible hydrocarbon chain (Scheme 1A).⁽²⁾ Cholesterol is practically insoluble in water. In biological systems it is mostly solubilized by incorporation in lipid membranes, bile salts, or with lipoproteins in blood. In cells, most of the cholesterol is located in the plasma membrane,⁽³⁾ where the hydrophobic region is embedded alongside the fatty-acid chains of lipids and the hydroxyl group points towards the water molecules surrounding the membrane (Scheme 1B).



Scheme 1. (A) Molecular structure of cholesterol. (B) Schematic representation of a bilayer composed of phosphoglycerolipids (red arrowhead) and cholesterol molecules (red arrow). Above a critical concentration for cholesterol, two-dimensional (2D) cholesterol crystalline domains are formed.

High levels of cholesterol are, however, pathological. They may result in the formation of two-dimensional (2D) crystalline cholesterol domains in cell membranes (Scheme 1B), and ultimately in the precipitation of cholesterol monohydrate crystals.^(4, 5) The precipitated cholesterol crystals can hardly be dissolved and therefore accumulate, leading to increased inflammatory response and to severe damage to the tissue.⁽⁵⁻⁷⁾ An unfortunate yet common outcome of this cholesterol deposition is atherosclerosis,⁽⁸⁻¹⁰⁾ a major cause of cardiovascular diseases and stroke.

The crystal structure of cholesterol.H₂O was determined by Craven only as late as 1976,⁽⁴⁾ possibly due to its noncentrosymmetric complexity: the space group is triclinic *P1*, with 8 independent cholesterol.H₂O units per cell, each containing 29 non-hydrogen atoms. We note, nonetheless, that the crystal structure has high pseudo-symmetry, which was taken advantage of by Craven for structure

determination. The habit of these cholesterol.H₂O crystals is usually rhomboid plates, by virtue of the crystal pseudo-symmetry and the layer-like molecular packing of cholesterol.

A different cholesterol.H₂O polymorph, with monoclinic structure, was identified in cholesterol nucleation from monolayers and multilayers at the air-water interface.^(11, 12) In this process, although the final multilayer structure is triclinic, the two leaflets of the first formed cholesterol bilayer are related by twofold screw symmetry in a 10×7.5 Å² rectangular unit cell. After its initial determination, this polymorph was also detected in supported lipid bilayers composed of lipid mixtures of cholesterol with phosphoglycerolipids and sphingolipids.⁽¹³⁻¹⁶⁾ 2D monoclinic crystalline domains, formed by segregation of cholesterol from the phospholipids, can either grow into three-dimensional (3D) crystals of the monoclinic polymorph⁽¹⁷⁾ or transform into the triclinic polymorph.^(12, 16) Surprisingly, the monoclinic polymorph was also identified in native bile solutions⁽¹⁸⁾ related to the formation of cholesterol gallstones, and in an atherosclerosis-related cell culture model,⁽¹⁹⁾ highlighting its relevance to cholesterol crystallization from a biological lipid-rich environment, such as that found in cell membranes and bile.

The three-dimensional structure of the monoclinic polymorph was determined making use of thin cholesterol films ranging from 1 to 3 bilayers, in a study on the nucleation of cholesterol at the air-water interface.⁽¹²⁾ Their structures were characterized via synchrotron grazing incidence X-ray diffraction (GIXD), a method that has been applied to molecular assemblies of crystalline films.^(20, 21) The single bilayer of cholesterol is of space group symmetry $p2_1$, namely the two leaflets are related by twofold screw symmetry.⁽¹¹⁾ The space group of the three bilayer film, with unit cell dimensions $a = 10.2$, $b = 7.6$, $c = 68.2$ Å, $\beta = 94.8^\circ$, was shown to be monoclinic $A2$ in a structure, determined to near-atomic resolution.^(20, 21) Details on the space group and structure elucidation at its basic level are presented in the Supporting Information (SI) §1.

Even with this structural information, ambiguities and unknowns remain. X-ray structure refinement of the monoclinic crystal, based on the intensities of the (hkl) reflections, yielded a reliability index $R = \sum |F_o^2(hkl) - F_c^2(hkl)| / \sum F_o^2(hkl) = 13.5\%$, where $F(hkl)$ is the X-ray structure factor of a particular diffraction peak and ‘o’ and ‘c’ refer to its observed and calculated values. This R index indicates an overall correct structure,⁽¹²⁾ but clearly further refinement is called for. A key issue that limits the refinement is that the arrangement of the water molecules and sterol-hydroxyl group, forming an H-bonded bilayer sandwiched between cholesterol bilayers, appears to be ill-determined. Beyond the ambiguous structural details, it is unclear why under some biological and/or chemical conditions cholesterol grows as the monoclinic polymorph to form 3D structures,^(17-19, 22) whereas under other conditions transformation into triclinic

plates occurs at an early stage.^(12, 16) Understanding this process appears to be relevant for clarifying critical stages in the pathological crystallization process.

We address these challenges by performing a comprehensive first principles computational study of both crystal polymorphs of cholesterol.H₂O, in particular that of the monoclinic form. We obtain a new, fully extended H-bonded network, comprising the sterol hydroxyl groups and water molecules in a structure akin to that of hexagonal ice. We show that the energy of the monoclinic and triclinic polymorphs is similar, strongly suggesting that kinetic and environmental effects play a significant role in determining polymorph nucleation. Furthermore, we find evidence in support of various O-H...O bonding motifs, in both polymorphs, that may result in structural disorder. We then rationalize what we believe is a single-crystal to single-crystal transformation of the monoclinic polymorph, on increased interlayer growth beyond that of a single cholesterol bilayer, interleaved by a water bilayer. We show that the ice-like structure is also relevant to the related cholestanol dihydrate (2H₂O) crystal. Finally, we posit a possible role for cholesterol esters in the crystallization of cholesterol.H₂O in pathological environments, with a composite of a bilayer of cholesteryl palmitate bound epitaxially as a nucleating agent to the monoclinic form of cholesterol.H₂O.

Results and Discussion

DFT optimization of the triclinic polymorph of cholesterol.H₂O. We begin our investigation with a dispersion-augmented DFT optimization of the known triclinic structure of the cholesterol.H₂O crystal (Fig. 1). As a starting point for geometry optimization, we use the structure originally determined by Craven,^(4, 23) based on the computational refinement of this structure by Frincu et al.,⁽²⁴⁾ in which sterol and water H atoms were introduced. There are, however, seven additional ways, beyond the motif originally reported by Frincu et al.,⁽²⁴⁾ in which the O-H...O bonds may be arranged in the H-bonding layer. In all arrangements, the basic H-bonding motif is composed of four octagons and four tetragons (Fig. 1C₁), but they differ in the relative orientation of the water molecules and the cholesterol OH group (see Fig. S2 for a detailed view of all arrangements). Therefore, crystal structure optimization was performed for all eight structures, with optimized structural parameters reported in Table S2.1 and average O...O H-bond distances listed in Table S2.2. Computed total energies for the proposed structural motifs, relative to the lowest energy motif, are given in Table S2.3. Importantly, all eight H-bonding networks result in very similar energies, suggesting that the crystal structure may be composed of a disordered

mixture of them. Furthermore, this structural disorder view agrees well with Craven's report,⁽⁴⁾ in which the H atoms participating in the H-bonded network were not found in electron density maps and therefore not included in the X-ray structure factor calculations. Therefore, Fig. 1C₂ presents the disordered-mixture arrangement of the hydrophilic region for these eight H-bonding networks, with partial occupation indicated by partial coloring of pertinent atoms.

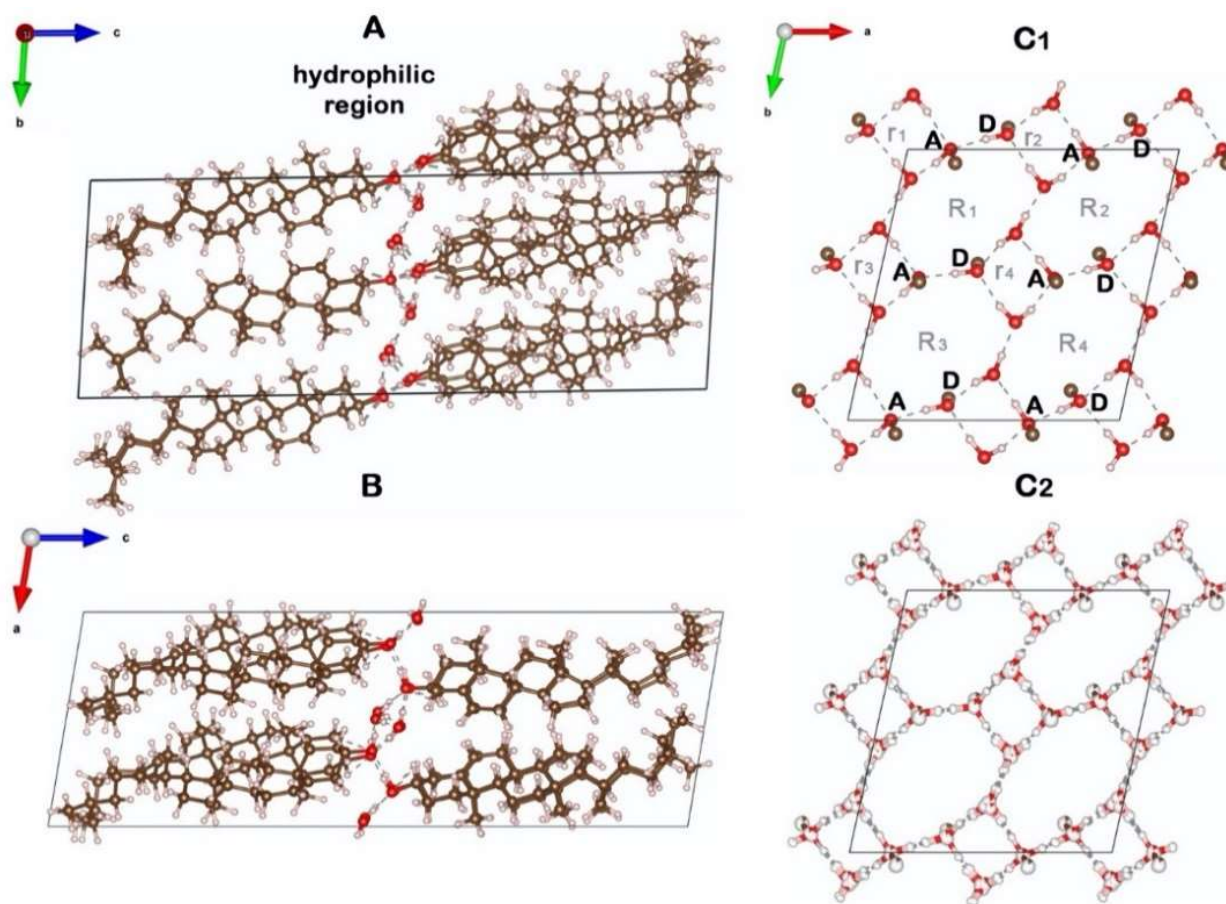


Fig. 1. Packing arrangement of the triclinic cholesterol.H₂O, viewed along the: *a*-axis (A), *b*-axis (B), and *c*-axis (C_{1,2}) for the hydrophilic region indicated in A. The atoms are color-coded in: white, H; brown, C; red, O. The different H-bonded rings in panel C₁ are labeled in grey by r_i and R_i , which refer to tetragons and octagons, respectively; the subscript $i=1 \dots 4$ designates the unique polygons of each type. For the sterol O atoms connected by H-bonds between the two hydroxyl groups, O atoms acting as a donor and acceptor are denoted by **D** and **A**, respectively. The arrangement in all panels, except for C₂, is for the lowest energy pseudopolymorph of the triclinic cholesterol.H₂O. The C₂ panel arrangement is of the hydrophilic region of the disordered mixture of the eight H-bonding networks with partial occupation indicated by partial coloring of pertinent atoms. OH \cdots O bonds are represented as grey dashed lines. The unit cell is indicated by a black rectangle.

DFT optimization of the monoclinic crystal structure of cholesterol.H₂O. To extend our investigation to the structure of the monoclinic cholesterol.H₂O polymorph, we based our initial guess on the structure reported by Solomonov et al.,⁽¹²⁾ with H atoms introduced to the cholesterol and water molecules. The obtained structure has eight cholesterol molecules in the unit cell, as shown in Fig. 2A and 2B₁ and contains two inequivalent molecules per asymmetric unit (labelled mol. A and mol. B in Fig. 2B₂). The *c* axis, which is ~ 70 Å long, contains two cholesterol bilayers related by internal twofold screw (2₁) symmetry, whereas the two cholesterol leaflets in each bilayer are related by twofold (2) symmetry.

In order to construct a favorable H-bonding network composed of (cholesterol)C-OH and H₂O molecules, in a 1:1 molar ratio, we need to modify the orientation in which the H atoms were originally introduced. To that end, we utilized a model that uses symmetry-related positions of the two asymmetric sterol O atoms, which belong to opposite leaflets of the bilayer (see SI, §3). These O atoms are separated by ~ 3 Å and H-bonded to each other to generate the positions of the symmetry-related water O atoms (Fig. S3). This model generates a somewhat distorted hexagonal arrangement of O-H \cdots O bonds, as in hexagonal ice, in bilayer form.

For dispersion-augmented DFT optimization based on the above motif, the monoclinic *A2* unit cell was reduced to a primitive unit cell that contains half the number of the molecular units. Both atomic coordinates and unit cell parameters were then fully optimized.¹ Finally, the conventional *A2* unit cell was reconstructed from the global minimum solution and the optimal H-bonded arrangement was found (See Methods for additional details). Overall, the computationally optimized structure of the monoclinic form given in Fig. 2 is very similar to the experimentally determined one. Specifically, the overall atomic structure of the tetracyclic part of the molecules, as well as the molecular tilt relative to the (001) plane, remained essentially unaltered. Some conformational changes occur at the hydrocarbon tail.

The optimized H-bonding motif is composed of two differently shaped fused hexagons, with average O \cdots O H-bond distances of 2.74 Å (Fig. 2C₂, labeled R₁), and 2.87 Å (Fig. 2C₂, labeled R₂). There are, however, three other ways in which the O-H \cdots O bonds may be arranged by interchanging the donor and acceptor roles of the sterol oxygens and hydrogen bonding orientation of the acceptor hydrogens (see Fig. S4). These three crystal structures were therefore also generated and optimized by DFT, and their energies are listed in Table S4.1, compared to that of the first generated motif. The optimized structural parameters thus determined are reported in Table S4.2. Two of these three H-bonding networks are almost as stable

¹ We note that following the relaxation process the system was first trapped in a local minimum, which was overcome by reorienting one H-atom to fit the model in Fig. S3.

as the original motif, suggesting that the crystal structure may be composed of a disordered mixture of three H-bonding networks. Importantly, $O\cdots O$ bond lengths of these two motifs are also close to the original motif, while in the fourth motif they differ from the other three (Table S4.2). The hydrophilic region arrangement of the disordered mixture of the three most-stable H-bonding networks, with partial occupation indicated by partial coloring of pertinent atoms, is shown in Fig. 2C₀.

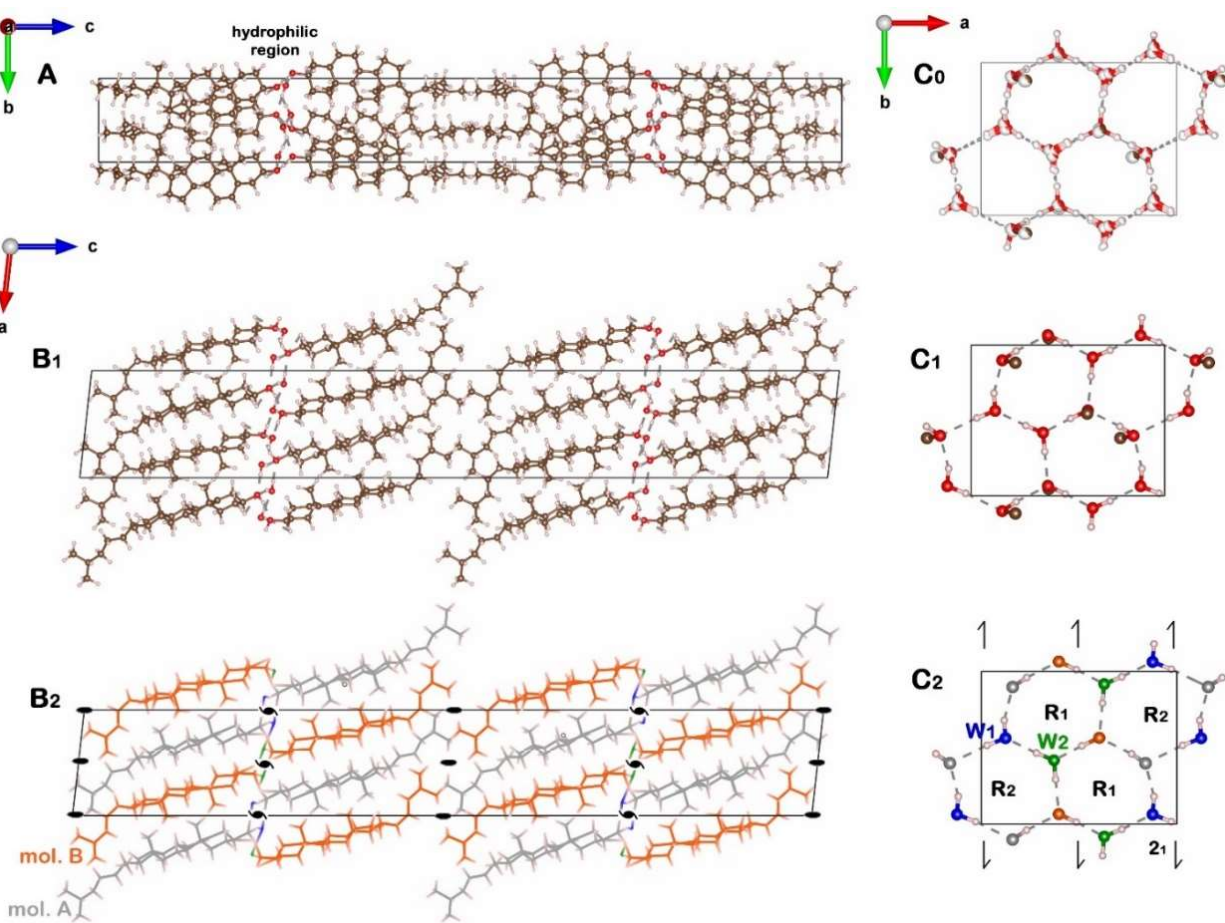


Fig. 2. Packing arrangement of the monoclinic cholesterol.H₂O unit cell, viewed along the: *a*-axis (A), *b*-axis (B_{1,2}), and *c*-axis (C_{0,1,2}) for the hydrophilic region indicated in A. For panels A, B₁, C₀, and C₁ the H, C, and O atoms are color-coded in white, brown, and red, respectively. Panels B₂ and C₂ present similar views as B₁ and C₁, respectively, but with different colors representing different symmetry-unrelated cholesterol and water molecules: grey, cholesterol molecule A (mol. A); orange, cholesterol molecule B (mol. B); blue (W₁) and green (W₂), water molecules. The two-fold and two-fold screw symmetry axes are shown in black. The hexagonal H-bonded rings in panel C₂ are labeled by R₁ and R₂. The arrangement in all the panels except for C₀ is for the lowest energy pseudopolymorph of the monoclinic cholesterol.H₂O. The C₀ panel arrangement is of the hydrophilic region of the disordered mixture of the three most stable H-bonding networks, with partial occupation indicated by partial coloring of pertinent atoms. OH \cdots O bonds are represented as grey dashed lines. The unit cell is indicated by a black rectangle.

Comparison of the computed two cholesterol.H₂O polymorphs with experiment. The total energy difference between the most stable pseudopolymorphs of the monoclinic and triclinic cholesterol monohydrate, as computed using pair-wise dispersion-augmented DFT (see Methods section), is found to be a small ~ 2.25 kcal/mol per molecule, in favor of the triclinic polymorph. While the computed energy ordering is consistent with experiment, it is important to keep in mind that it is at the limit of accuracy of the computational approach.^(25, 26) Furthermore, it may be washed out by entropic effects. Therefore, it is indeed reasonable that both polymorphs are accessible experimentally. Further gas-phase calculations of cholesterol molecules taken from the bulk (see Fig. S5) reveal that the difference in energy between isolated (gas-phase) cholesterol molecules taken from the bulk of either polymorph without further relaxation is an insignificant ~ 0.3 kcal/mol in favor of the triclinic form.² Therefore, the computed energy difference arises entirely from intermolecular interactions.

The optimized structural parameters of the most stable pseudopolymorphs of the monoclinic and triclinic cholesterol.H₂O are given in Table 1. The results reveal that the computed lattice parameters are consistently smaller than the experimentally determined ones, such that the computed unit cell volume is smaller than the experimental one by $\sim 9\%$. This difference between experiment and theory is larger than that typically found with pair-wise-dispersion augmented DFT for smaller, more rigid molecules (usually $< 3\%$,^(25, 26) although larger volume discrepancies of $\sim 5\%$ have been reported for flexible molecules).⁽²⁶⁾ To test whether this is a consequence of the level of theory used, we performed further optimization using the more advanced many body dispersion (MBD) approach, with⁽²⁷⁾ and without⁽²⁸⁾ non-local corrections (see Methods section), for the monoclinic polymorph. This, however, did not result in any significant improvement of agreement with experiment (see Table S6).

² Similarly, the difference in energy of the isolated, infinite water layer (see Methods for details) is ~ 0.5 kcal/mol per molecule, with the arrangement of the triclinic form being slightly more stable.

Table 1. Comparison of experimental and calculated unit cell parameters (in Å, degrees, and Å³), derived via DFT for the triclinic and monoclinic forms of cholesterol.H₂O, shown. Experimental parameters for the triclinic and monoclinic structures were taken from Craven^(4, 23) and Solomonov et al.,⁽¹²⁾ respectively, and we compare them to the corresponding lowest energy H-bonding motifs optimized by DFT.

	method	<i>a</i>	<i>b</i>	<i>c</i>	α	β	γ	V
triclinic	SC-XRD ⁴	12.39	12.41	34.36	91.9	98.1	100.8	5128.2
	PBE-TS	11.85	11.95	34.16	92.1	98.8	102.0	4663.3
	Δ in %	4.34	3.73	0.60	0.20	0.70	1.19	9.07
monoclinic	GIXD ²³	10.15	7.57	68.20	90.0	94.8	90.0	5222.0
	PBE-TS	9.63	7.46	66.90	90.0	96.3	90.0	4778.7
	Δ in %	5.09	1.45	1.90	0.00	1.62	0.00	8.49

An alternate explanation for this discrepancy is that cholesterol is characterized by large thermal motion at room temperature.^(4, 23) Specifically, the proposed trigonal lattice symmetry and packing arrangement of the cholesterol crystalline monolayer on water⁽¹¹⁾ has been interpreted in terms of pronounced libration about the long molecular axis. This molecular motion is high enough to exclude contribution of the exocyclic hydrocarbon moiety to the Bragg rod intensity profile as measured by GIXD.⁽¹²⁾ Thus, libration of the molecules around its long axis, coupled with motion of the exocyclic hydrocarbon moiety, may induce increased intralayer packing distances in the monoclinic and triclinic polymorphs. In this view, the discrepancy between theory and experiment than arises mostly from the comparison of room temperature experimental data with 0 K computational data. To test that, we compare the computed data against (*hkl*) (111) and (200) *d*-spacings, deduced from the electron diffraction (ED) measurements of Weihs et al.,⁽¹⁸⁾ which correspond to a temperature of 90 K, and from the GIXD data of Solomonov et al.⁽¹²⁾ taken at 278 K. Overall this comparison, summarized in Fig. 3 and Table S7, shows a reduction of ~3.0-5.5% in the *d*-spacing with decreasing temperature, which would eliminate much of the remaining discrepancy.

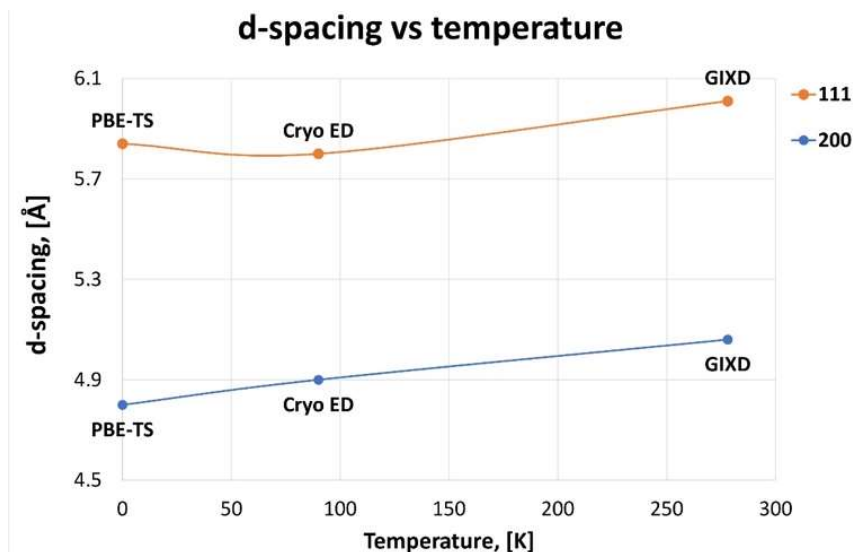


Fig. 3. Temperature dependence of the d -spacing of monoclinic cholesterol.H₂O, measured by electron diffraction (ED)⁽¹⁸⁾ and grazing incidence X-ray diffraction (GIXD),⁽¹²⁾ and compared to calculations at the PBE-TS level of theory.

We note that we have also compared the theoretical growth morphologies of the triclinic and monoclinic structures, determined using interatomic potential energy computations (see Methods section for details). The results are given in the SI (§8) and again reveal, by and large, a match to that of the observed morphologies of crystals grown in solution.

Taken together, the above comparison validates the computational approach, such that we can draw new insights from further calculations.

Symmetry change in cholesterol multi-bilayers of the monoclinic form. As already mentioned in the Introduction, the two cholesterol leaflets are related by twofold screw symmetry for a single bilayer at the air-water interface or if hydrated at both sides of the film. As a triple bilayer crystal on the water surface, however, the cholesterol leaflets, in contact via their hydrocarbon tails, are related by twofold symmetry.⁽¹²⁾ At first sight, this is surprising since in general the twofold screw symmetry element lends itself to better molecular packing than twofold symmetry.⁽²⁹⁾

To rationalize this, we generated a series of hypothetical *bulk* $P2_1$ crystal structures of cholesterol.H₂O (Fig. S9.1), by first replacing the twofold axes of the $A2$ polymorph by twofold screw axes. This change in space group was followed by offsetting adjacent cholesterol bilayers along the a -axis, but maintaining the original H-bonded bilayer system, across which the corresponding cholesterol layers are related by twofold screw symmetry. The DFT-computed energy profile of this series of generated crystal structures

(Fig. S9.2) revealed that the crystal structure with no offsetting of the adjacent cholesterol bilayers along the a -axis to be the most stable. We then compared this hypothetical bulk $P2_1$ structure of cholesterol.H₂O, after relaxation, with the above-obtained $A2$ polymorph. The comparison revealed that the energy difference between the two structures, at the MBD level of theory, is ~ 32.8 kcal/mol per molecule in favor of $A2$, in agreement with the experimental observation.

Naturally, the next question to examine is the energetics of a *single* cholesterol bilayer, because the symmetry of this bilayer at the air-water interface or hydrated at opposite sides is $p2_1$. We therefore generated a bilayer in which the two leaflets are related by twofold screw symmetry, as opposed to a twofold axis, given as at the water surface or as hydrated at both sides, with a $p2_1$ crystal symmetry (Fig. S10). The computed energy difference between the relaxed structures of such $p2_1$ bilayers, compared to bilayers with the original $p2$ symmetry, was found to be ~ 0.85 Kcal/mol per molecule and ~ 1.08 kcal/mol per molecule, for a cholesterol bilayer in vacuum and a bilayer hydrated from both sides, respectively, with $p2_1$ being consistently more stable.

The computed stability of the $p2_1$ bilayer, but of the $A2$ bulk, fully agrees with experiment, and furthermore suggests a single-crystal to single-crystal transformation. This is consistent with the similarity of the Bragg rod data of the one, two, and three cholesterol bilayers (see Fig. S11).

Generality of the ice-like motif and proposed crystal structure of cholestanol.2H₂O. Clearly, the identification of an ice-like motif (Fig. 4A) plays a major role in the above considerations for the monoclinic polymorph (Fig. 4B). This arrangement is quite distinct from the hydrogen-bonded network in the triclinic system (Fig. 4C), although in both each oxygen atom participates in three H-bonds of a proton-disordered network. The ice-like network can be rationalized in view of a partial lattice and stereochemical match. Specifically, the monoclinic motif incorporates a pseudo-centered $7.5 \times 5 \text{ \AA}^2$ sub-lattice. Indeed, ice nucleation was promoted via monolayers of long-chain aliphatic alcohols, which pack in a two-dimensional $7.5 \times 5 \text{ \AA}^2$ lattice and whose OH groups are also arranged in a (pseudo) centered cell,^(30, 31) as in the layer structure of hexagonal ice itself.

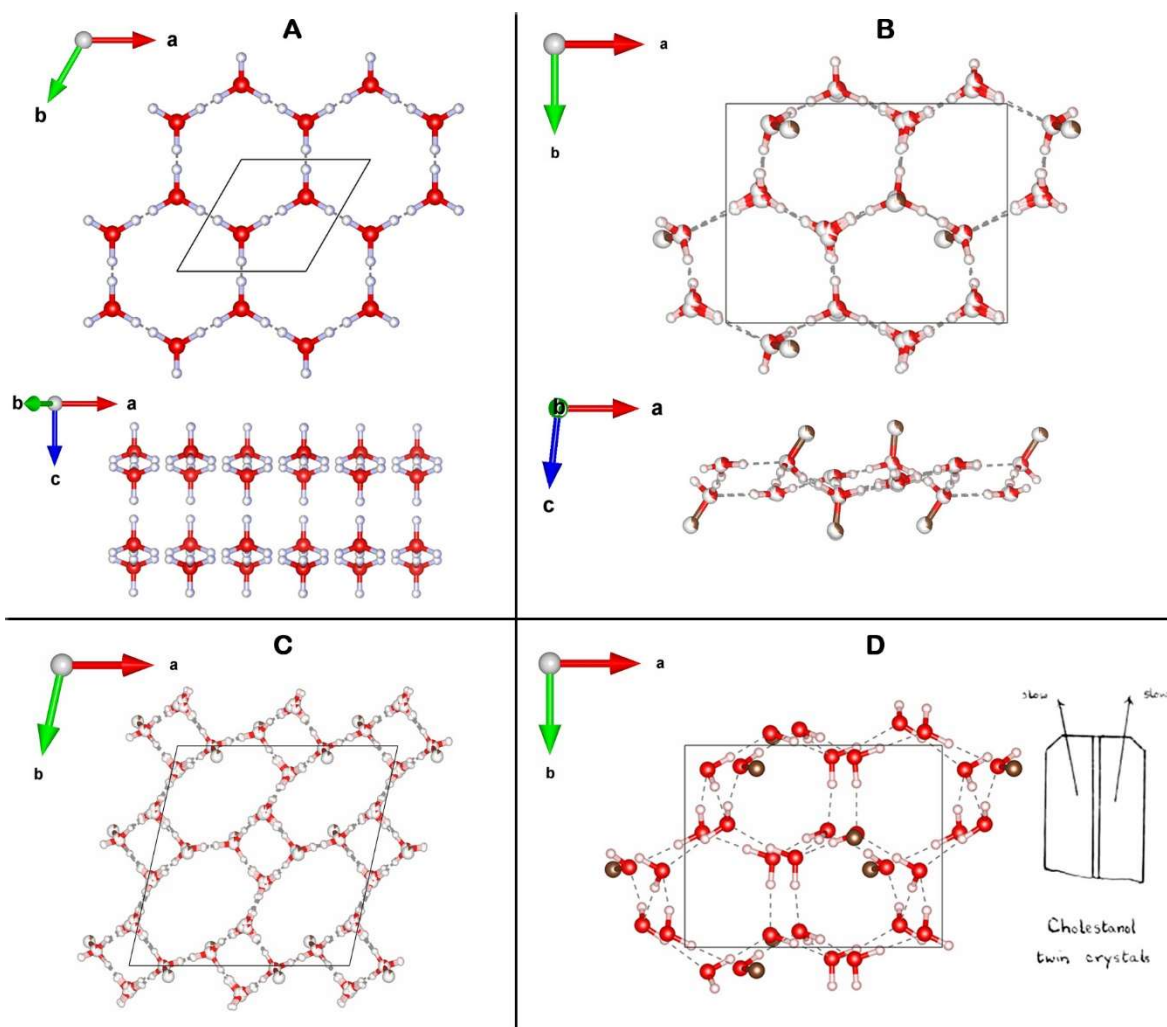


Fig. 4. Schematic view of the H-bonded bilayers of cholesterol.H₂O and cholestanol.2H₂O. Top and side views of: (A) The hexagonal H-bonding bilayer in the structure of hexagonal ice⁽³²⁾ and (B) The disordered mixture of the three most stable H-bonding networks of the monoclinic cholesterol, with partial occupation indicated by partial coloring of pertinent atoms; (C) The disordered mixture of the eight H-bonding networks of the triclinic cholesterol, with partial occupation indicated by partial coloring of pertinent atoms; (D) The model H-bonded network of cholestanol. Also shown a drawing of cholestanol crystals, taken from the PhD Thesis of D. Hodgkin (1937).⁽³³⁾ The two crystals are elongated, twinned about the [010] direction, and show mainly the (001) face with small (100), (010) and (110) faces. Reproduced by permission of the Hodgkin family.

It is therefore important to examine whether the above-suggested ice-like motif is unique to the monoclinic structure of cholesterol.H₂O, or is more general. To assess that, we considered the cholestanol.2H₂O⁽³³⁾ crystal, a close relative of cholesterol.^(33, 34) Importantly, the 10×7.5 Å² monoclinic motif is predominant in the two- and three-dimensional crystals of various cholesterol-type molecules.⁽¹²⁾ In particular, the unit cell of cholestanol dihydrate, reported in the PhD thesis by D. Hodgkin⁽³³⁾ to be of triclinic *P1* symmetry, can be transformed to a pseudo *A2* cell similar to that of monoclinic

cholesterol.H₂O, but with a *c*-axis longer by approximately 6 Å, which is consistent with a double ice-like bilayer (Table 2).^(30, 31, 34) To test this, we generated the model packing by inserting two additional H-bonded bilayers to the monoclinic structure of cholesterol.H₂O, converting cholesterol to cholestanol, and optimizing the crystal structure by DFT. A stable structure with *A2* symmetry and dimensions close to experiment (Table 2) was indeed found, lending further important support to the suggested ice-like structure and demonstrating its generality. The H-bonding motif and drawings of the associated crystal shape are given in Fig. 4D, with the energy-minimized structure provided in Fig. S13.

Table 2. Summary of structural parameters of cholestanol.2H₂O (in Å, degrees, and number of molecules per asymmetric unit, *n*).

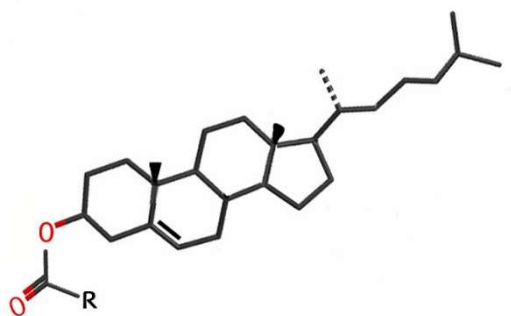
	<i>a</i>	<i>b</i>	<i>c</i>	α	β	γ	Space group	<i>n</i>
Triclinic cell ^(33, 35)	9.79	7.76	36.8	83.0	106.0	88.5	<i>P1</i>	4
Triclinic, transformed to pseudo <i>A2</i> ³	9.8	7.8	73.8	89.1	106.1	88.5	pseudo <i>A2</i>	2
DFT optimized <i>A2</i>	9.52	7.44	75.14	90.0	95.3	90.0	<i>A2</i>	2

Model of induced nucleation of monoclinic cholesterol.H₂O via a bilayer of cholesteryl palmitate.

Last but not at all least, we reach the important question of the nucleation and growth of cholesterol crystals in atherosclerosis. In addition to cholesterol crystals, most atherosclerotic plaques develop calcifications of apatite (calcium phosphate) crystals. Lonsdale published a paper in 1968,⁽³⁶⁾ in which she laid out possible epitaxial matches and consequently epitaxial growth of crystals in gallstones. Could the same apply to atherosclerosis? We consider here the possibility that epitaxy may play a role in the nucleation of cholesterol monohydrate crystals, not in relation to apatite, but to cholesterol esters. Cholesterol crystal deposition occurs in atherosclerosis when cholesterol reaches super-saturation in the lipid environment because of the accumulation of unesterified cholesterol, following hydrolysis of cholesteryl esters. The hydrolysis of cholesteryl esters is associated with the breakdown of lipid bodies, inside lysosomal compartments or at extracellular locations following cell death.^(8, 37, 38) The major cholesterol esters found in atherosclerotic lesions are cholesteryl palmitate, oleate, and linoleate^(5, 39) (Scheme 2). Of these three molecules, the palmitate crystallizes in the rectangular 10×7.5 Å² cholesterol-type monoclinic motif (as does the related myristate derivative, see SI §1); a crystal structure of the

³ Transformation of the primitive cell (*a, b, c*) of cholestanol.2H₂O to an *A*-centered cell (*a*₁, *b*₁, *c*₁), where *c*₁ = 2*c* - *b*. This transformation is described in the SI of the article by Solomonov et al.⁽¹²⁾

linoleate has not been reported, perhaps because of its doubly unsaturated chain; the oleate derivative has a crystal structure with no resemblance to that of monoclinic cholesterol.H₂O.⁽⁴⁰⁾



Scheme 2. Cholesteryl esters. The palmitate derivative has a saturated aliphatic chain (C₁₆H₃₁); the chain of the oleate derivative (C₁₈H₃₃) contains a C=C double bond with a *cis* configuration; the linoleate has a chain (C₁₈H₃₁) with two C=C double bonds, both with *cis* configuration.

According to surface pressure-area isotherms and grazing incidence X-ray diffraction measurements, cholesteryl tridecanoate (C₁₃H₂₅), palmitate (C₁₆H₃₁), and stearate (C₁₈H₃₅), each containing saturated aliphatic chains, self-assemble into crystalline single bilayer films in a unit cell of 10×7.5 Å² at the air-water interface, where the two layers are interdigitated across their hydrocarbon ester chains.⁽⁴¹⁾ The cholesteryl moieties of the bilayer form a structure akin to the layer of cholesterol molecules in its monoclinic polymorph. Given the ease with which cholesteryl palmitate forms a single crystalline bilayer at the air-water interface,⁽⁴¹⁾ we propose a model by which the palmitate derivative forms a crystalline bilayer inside lipid bodies or lysosomal compartments and acts as a nucleating agent of the monoclinic cholesterol form. We therefore set out to examine, by DFT, the possibility of epitaxial nucleation of cholesterol.H₂O onto the cholesteryl surface of a cholesteryl palmitate bilayer. Making use of the crystal structure of cholesteryl myristate,⁽⁴²⁾ we have been able to construct a model of the packing arrangement of a bilayer of cholesteryl palmitate, bound epitaxially as a nucleating agent to the monoclinic form of cholesterol.H₂O (Fig. 5). We have been able to converge this structure to atomic forces smaller than 10⁻² eV/Å, meaning that it is substantially stable, and therefore supporting the model hypothesis.

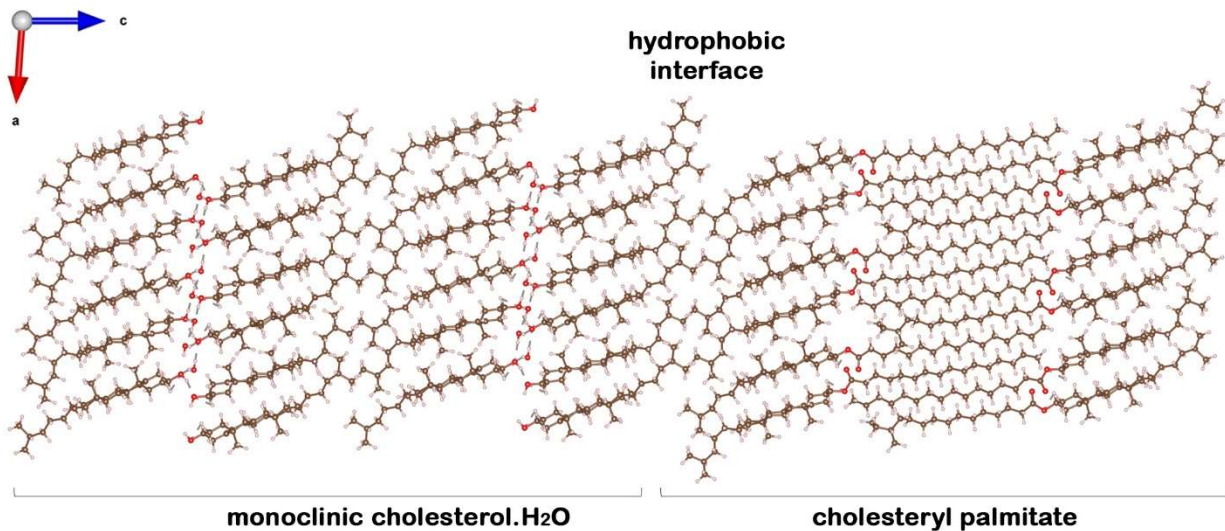


Fig. 5. Simulation of a composite crystal, in which the cholesteryl palmitate bilayer is epitaxially bound to monoclinic cholesterol molecules across twofold axes. As a bilayer, the cholesteryl palmitate is found to be sufficiently stable and could therefore nucleate the monoclinic crystals of cholesterol.H₂O by epitaxy.

Transformation from the monoclinic to the triclinic form of cholesterol.H₂O. Importantly, 2D crystals of cholesterol bilayers hydrated at both sides segregating from mixed bilayers with phospholipids always appear in the monoclinic polymorph,⁽¹³⁻¹⁶⁾ and only later transform into the triclinic polymorph.⁽¹⁶⁾ This transformation has been modeled as a single-crystal to single-crystal transition, at least in its initial stages.⁽¹²⁾ The greater stability of the triclinic polymorph at room temperature may be explained in terms of it having more degrees of freedom to accommodate thermal motion of the exocyclic groups. The monoclinic structure contains two symmetry-unrelated cholesterol molecules with different conformations of their exocyclic moieties, whereas the triclinic polymorph contains essentially four non-symmetry related molecules with different exocyclic group conformations. However, as was found experimentally,⁽¹¹⁻¹⁵⁾ as a bilayer on water, or if hydrated from both sides, the monoclinic arrangement is more stable.

The rate of the transformation between the polymorphs depends on the phospholipid environment.^(22, 43) Thus, as an example, only macroscopic 3D triclinic crystals are observed associated with sphingomyelin-containing mixed bilayers, whereas the initial monoclinic crystals are retained and developed when they form from DPPC-containing mixed bilayers.⁽²²⁾ Monoclinic helical crystals formed from solutions with bile acids are also relatively long-lived, before transformation to the more stable triclinic polymorph.⁽¹⁸⁾ Helical triclinic crystals of cholesterol have also been characterized by synchrotron X-ray diffraction, yielding unit cell dimensions similar to that of the thermodynamically stable polymorph

of cholesterol.H₂O, but with a *c* axis three times as long.⁽⁴⁴⁾ In the above systems, the lipid environment determines the rate of the transformation. Therefore, while cholesterol crystals found in atherosclerotic plaques were exclusively identified as the triclinic polymorph,^(5,45) it stands to reason that they could have formed as monoclinic crystals, having had years to transform prior to extraction. In this respect, we note that a model has been presented above of the induction of the monoclinic form via an epitaxial fit to a bilayer of cholesteryl palmitate, a molecule present in atherosclerotic lesions. The abundance of needle-like crystals in mature plaques is tantalizing, in suggesting that this needle-like morphology may be a vestige of the initial formation of the crystals in the monoclinic polymorph. This conclusion is further supported by the observation of monoclinic helical crystals in freshly fixed macrophage cells (the cholesterol scavengers in atherosclerosis), to which cholesterol was administered in excess.⁽²²⁾ It would be interesting to determine whether the relative ease of formation of the monoclinic domains within the bilayers may be related to the relative advantage of the 10×7.5 Å² unit cell, witnessed by its occurrence in many cholesterol derivatives, relative to the 12×12 Å² unit cell.

Conclusions

In conclusion, we presented a comprehensive computational study of the two crystal polymorphs of cholesterol.H₂O, with an emphasis on the lesser-known monoclinic one. Using first principles calculations based on dispersion-augmented DFT, we confirmed the known features of the experimentally determined structures. Furthermore, we refined the structure of the monoclinic polymorph by obtaining a new, fully extended H-bonded network, comprising the sterol hydroxyl groups and water molecules in an arrangement akin to that of hexagonal ice. We further suggested that this network may exist in related structures, notably that of cholestanol.2H₂O. The total energy of this newly refined monoclinic form was found to be similar to that of the triclinic one, suggesting that kinetic and environmental effects may play an important role in determining the polymorphic nucleation of cholesterol. We have also rationalized a single-crystal to single-crystal transformation of the monoclinic form on increased interlayer growth from one to several cholesterol bilayers. Finally, we examined the relevance of our findings to pathological cholesterol.H₂O crystallization via lipid bodies containing the cholesteryl palmitate ester and from lipid membranes. We have found an epitaxial match between the cholesteryl surface of a single bilayer of the ester and the corresponding surface of monoclinic cholesterol.H₂O, leading to its proposed nucleation.

Then we discussed how our findings lend support to and partially rationalize the observation of nucleation of the monoclinic structure from lipid membranes, followed by transformation to the triclinic counterpart.

Methods

Structure construction. The crystal structure of the monoclinic cholesterol monohydrate was taken from Solomonov et al.,⁽¹²⁾ with hydrogen atoms added using Materials studio 6.1.⁽⁴⁶⁾ The unit-cell was then transformed to a primitive cell, containing half the atoms, with a single water-hydroxyl layer. We derived the primitive cell of monoclinic cholesterol using the phonopy package,⁽⁴⁷⁾ which determines the transformation matrix from the input unit cell to the primitive one, M_p . For the monoclinic $A2$ unit cell, M_p based on the $A2$ conventional unit cell is given by:

$$M_p = \begin{pmatrix} 0 & 0 & 1 \\ 0.5 & -0.5 & 0 \\ 0.5 & 0.5 & 0 \end{pmatrix},$$

These values agree with those displayed in Table 5.1 of the International Tables for Crystallography.⁽⁴⁸⁾ The primitive cell of cholestanol dihydrate was derived in a similar matter using same transformation matrix.

For vacuum calculations of the $p2_1$ and $p2$ structures and the composite crystal, a layer of vacuum of ~ 10 Å was added to cut the periodicity in the c -axis. To study the contribution of inter- and intra-molecular forces on the molecular packing of cholesterol monohydrate crystals, isolated single cholesterol molecules of the triclinic and monoclinic pseudopolymorphs the vacuum spacing was at least 10 Å in all three axes. The same vacuum spacing was also applied to the isolated infinite H-bonded networks, with cholesterol C atom connected to the cholesterol hydroxyl (OH) group replaced with H.

Molecular structures were visualized using the VESTA, a three-dimensional visualization system for electronic and structural analysis.⁽⁴⁹⁾

Density Functional theory (DFT) calculations. Electronic structures, total energies, and geometries were calculated by solving the Kohn-Sham equations of DFT within the generalized gradient approximation (GGA), using the Perdew, Burke and Ernzerhof (PBE) exchange-correlation functional.⁽⁵⁰⁾ The total energy was augmented by Tkatchenko-Scheffler van der Waals (TS-vdW) pair-wise dispersive terms.⁽⁵¹⁾ Most of the calculations were carried out using version 5.4.4 of the Vienna Ab Initio Simulation Package (VASP)⁽⁵²⁾ plane wave basis code.^(53, 54), where ionic cores are described by the projected

augmented wave (PAW) method.^(52,55) A plane wave energy cutoff of 920 eV was used in all calculations. Further calculations of the composite crystal, as well as MBD⁽²⁷⁾ and MBD-NL⁽²⁸⁾ based calculations,^(27,28) were performed using the Fritz Haber Institute *ab initio* molecular simulations (FHI-aims) package.⁽⁵⁶⁾ FHI-aims is an all-electron, full-potential electronic structure code utilizing numeric atom-centered basis functions for its electronic structure calculations, which we used to speed up testing and address large system computations. We employed the 'intermediate' settings using the *tier1* and some of the *tier2* basis functions. 'Tight' settings, which include the larger *tier2* basis sets and considered to result in converged conformational energy differences at a level of a few meV,⁽⁵⁶⁾ were used to test the basis set convergence. The Brillouin zone was sampled using a Gamma-centered Monkhorst–Pack *k*-point grid⁽⁵⁷⁾ of 3×3×1 and 2×2×7 for the triclinic and monoclinic structures, respectively, and 2×2×8 for cholesterol dihydrate. Atomic forces in the system were relaxed to 10⁻⁴ eV/Å and stress was relaxed to 10⁻³ kB.

Acknowledgments. This research was supported by the Binational Science Foundation (Grant 2013045). L.A. is the incumbent of the Dorothy and Patrick Gorman Professorial Chair of Biological Ultrastructure, and L.K. is the incumbent of the Aryeh and Mintzi Katzman Professorial Chair at the Weizmann Institute of Science. We thank Dr. Fabio Beghi (Università degli Studi di Milano) for participation in the initial DFT optimization of the monoclinic form of cholesterol monohydrate. We thank Prof. Alexandre Tkatchenko (University of Luxembourg) and Prof. Volker Blum (Duke University) for helpful discussions.

References

1. B Alberts, et al., *Molecular Biology of the Cell*. (New York: W. W. Norton & Company), 6th edition, (2014).
2. BM Craven, The physical chemistry of lipids – from alkanes to phospholipids in *Handbook of Lipid Research*, eds. DJ Hanahan, DM Small. (Plenum Press) Vol. 4, pp. 149–182 (1986).
3. G Van Meer, DR Voelker, GW Feigenson, Membrane lipids: where they are and how they behave. *Nat Rev Mol Cell Biol* **9**, 112–124 (2008).
4. BM Craven, Crystal structure of cholesterol monohydrate. *Nature* **260**, 727–729 (1976).
5. DM Small, George Lyman Duff memorial lecture. Progression and regression of atherosclerotic lesions. Insights from lipid physical biochemistry. *Arteriosclerosis: An Official Journal of the American Heart Association, Inc.* **8**, 103–129 (1988).
6. K Rajamäki, et al., Cholesterol crystals activate the NLRP3 inflammasome in human macrophages: a novel link between cholesterol metabolism and inflammation. *PLoS One* **5**, e11765 (2010).
7. GS Abela, Cholesterol crystals piercing the arterial plaque and intima trigger local and systemic inflammation. *J Clin Lipidol* **4**, 156–164 (2010).
8. HS Kruth, Lipoprotein cholesterol and atherosclerosis. *Curr Mol Med* **1**, 633–653 (2001).
9. W Insull Jr, GE Bartsch, Cholesterol, triglyceride, and phospholipid content of intima, media, and atherosclerotic fatty streak in human thoracic aorta. *J Clin Invest* **45**, 513–523 (1966).
10. HS Kruth, Localization of unesterified cholesterol in human atherosclerotic lesions. Demonstration of filipin-positive, oil-red-O-negative particles. *Am J Pathol* **114**, 201–208 (1984).
11. H Rapaport, et al., Cholesterol monohydrate nucleation in ultrathin films on water. *Biophys J* **81**, 2729–2736 (2001).
12. I Solomonov, MJ Weygand, K Kjaer, H Rapaport, L Leiserowitz, Trapping crystal nucleation of cholesterol monohydrate: relevance to pathological crystallization. *Biophys J* **88**, 1809–1817 (2005).
13. R Ziblat, K Kjaer, L Leiserowitz, L Addadi, Structure of cholesterol/lipid ordered domains in monolayers and single hydrated bilayers. *Angew Chem Int Ed* **48**, 8958–8961 (2009).
14. R Ziblat, L Leiserowitz, L Addadi, Crystalline domain structure and cholesterol crystal nucleation in single hydrated DPPC:cholesterol:POPC bilayers. *J Am Chem Soc* **132**, 9920–9927 (2010).
15. R Ziblat, L Leiserowitz, L Addadi, Crystalline lipid domains: Characterization by X-ray diffraction and their relation to biology. *Angew Chem Int Ed* **50**, 3620–3629 (2011).

16. R Ziblat, I Fargion, L Leiserowitz, L Addadi, Spontaneous formation of two-dimensional and three-dimensional cholesterol crystals in single hydrated lipid bilayers. *Biophys J* **103**, 255–264 (2012).
17. N Varsano, I Fargion, SG Wolf, L Leiserowitz, L Addadi, Formation of 3D cholesterol crystals from 2D nucleation sites in lipid bilayer membranes: implications for atherosclerosis. *J Am Chem Soc* **137**, 1601–1607 (2015).
18. D Weihs, et al., Biliary cholesterol crystallization characterized by single-crystal cryogenic electron diffraction. *J Lipid Res* **46**, 942–948 (2005).
19. N Varsano, et al., Two polymorphic cholesterol monohydrate crystal structures form in macrophage culture models of atherosclerosis. *PNAS* **115**, 7662–7669 (2018).
20. I Kuzmenko, et al., Design and characterization of crystalline thin film architectures at the air-liquid interface: Simplicity to complexity. *Chem Rev* **101**, 1659–1696 (2001).
21. D Jacquemain, et al., Two-dimensional crystallography of amphiphilic molecules at the air-water interface. *Angew Chem Int Ed* **31**, 130–152 (1992).
22. N Varsano, et al., The effect of the phospholipid bilayer environment on cholesterol crystal polymorphism. *ChemPlusChem* **84**, 338–344 (2019).
23. BM Craven, Pseudosymmetry in cholesterol monohydrate. *Acta Cryst B* **35**, 1123–1128 (1979).
24. MC Frincu, SD Fleming, AL Rohl, JA Swift, The epitaxial growth of cholesterol crystals from bile solutions on calcite substrates. *J Am Chem Soc* **126**, 7915–7924 (2004).
25. L Kronik, A Tkatchenko, Understanding molecular crystals with dispersion-inclusive density functional theory: Pairwise corrections and beyond. *Acc Chem Res* **47**, 3208–3216 (2014).
26. J Hoja, et al., Reliable and practical computational description of molecular crystal polymorphs. *Sci Adv* **5**, eaau3338 (2019).
27. A Ambrosetti, AM Reilly, RA DiStasio Jr, A Tkatchenko, Long-range correlation energy calculated from coupled atomic response functions. *J Chem Phys* **140**, 18A508 (2014).
28. J Hermann, A Tkatchenko, Density functional model for van der Waals interactions: Unifying many-body atomic approaches with nonlocal functionals. *Phys Rev Lett* **124**, 146401 (2020).
29. AL Kitaigorodsky, *Molecular Crystals and Molecules*. (Academic Press, Inc.), (1973).
30. M Gavish, R Popovitz-Biro, M Lahav, L Leiserowitz, Ice nucleation by alcohols arranged in monolayers at the surface of water drops. *Science* **250**, 973–975 (1990).
31. I Weissbuch, M Lahav, L Leiserowitz, Toward stereochemical control, monitoring, and understanding of crystal nucleation. *Cryst Growth Des* **3**, 125–150 (2003).

32. SW Peterson, HA Levy, A single-crystal neutron diffraction study of heavy ice. *Acta Crystallogr* **10**, 70–76 (1957).
33. DM Crowfoot, Ph.D. thesis (Universities of Oxford and Cambridge) (1937).
34. R Popovitz-Biro, et al., Induced freezing of supercooled water into ice by self-assembled crystalline monolayers of amphiphilic alcohols at the air-water interface. *J Am Chem Soc* **116**, 1179–1191 (1994).
35. JD Bernal, D Crowfoot, I Fankuchen, X-ray crystallography and the chemistry of the steroids. Part I. *Philos Trans R Soc A* **239**, 135–182 (1940).
36. K Lonsdale, Human stones: limited studies give some details of composition, rates of growth, distribution, and possible causes. *Science* **159**, 1199–1207 (1968).
37. RK Tangirala, FH Mahlberg, JM Glick, WG Jerome, GH Rothblat, Lysosomal accumulation of unesterified cholesterol in model macrophage foam cells. *J Biol Chem* **268**, 9653–9660 (1993).
38. I Tabas, WJ Rosoff, GC Boykow, Acyl coenzyme a: cholesterol acyl transferase in macrophages utilizes a cellular pool of cholesterol oxidase-accessible cholesterol as substrate. *J Biol Chem* **263**, 1266–1272 (1988).
39. B Lundberg, Chemical composition and physical state of lipid deposits in atherosclerosis. *Atherosclerosis* **56**, 93–110 (1985).
40. Q Gao, BM Craven, Conformation of the oleate chains in crystals of cholesteryl oleate at 123 k. *J Lipid Res* **27**, 1214–1221 (1986).
41. C Alonso, et al., Self-assembly of crystalline films of interdigitated long-chain cholesteryl esters at the air- water interface. *J Phys Chem B* **105**, 8563–8568 (2001).
42. BM Craven, GT DeTitta, Cholesteryl myristate: structures of the crystalline solid and mesophases. *Journal of the Chemical Society, Perkin Transactions 2*, 814–822 (1976).
43. FM Konikoff, DE Cohen, MC Carey, Phospholipid molecular species influence crystal habits and transition sequences of metastable intermediates during cholesterol crystallization from bile salt-rich model bile. *J Lipid Res* **35**, 60–70 (1994).
44. B Khaykovich, et al., Structure of cholesterol helical ribbons and self-assembling biological springs. *PNAS* **104**, 9656–9660 (2007).
45. SS Katz, GG Shipley, DM Small, Physical chemistry of the lipids of human atherosclerotic lesions. Demonstration of a lesion intermediate between fatty streaks and advanced plaques. *J Clin Invest* **58**, 200–211 (1976).

46. *Materials Studio 6.1*, Accelrys Inc., San Diego, CA, (2012).
47. A Togo, I Tanaka, First principles phonon calculations in materials science. *Scr Mater* **108**, 1–5 (2015).
48. H Arnold, Transformations of the coordinate system (unit-cell transformations) in *International Tables for Crystallography Volume A: Space-group symmetry*. (Springer), pp. 78–85 (2006).
49. K Momma, F Izumi, VESTA 3 for three-dimensional visualization of crystal, volumetric and morphology data. *J Appl Crystallogr* **44**, 1272–1276 (2011).
50. JP Perdew, K Burke, M Ernzerhof, Generalized gradient approximation made simple. *Phys Rev Lett* **77**, 3865–3868 (1996).
51. A Tkatchenko, M Scheffler, Accurate molecular van der Waals interactions from ground-state electron density and free-atom reference data. *Phys Rev Lett* **102**, 073005(4) (2009).
52. G Kresse, J Hafner, *Ab initio* molecular dynamics for liquid metals. *Phys Rev B* **47**, 558–561 (1993).
53. WA Al-Saidi, VK Voora, KD Jordan, An assessment of the vdW-TS method for extended systems. *J Chem Theory Comput* **8**, 1503–1513 (2012).
54. T Bucko, S Lebègue, J Hafner, JG Angyan, Tkatchenko-Scheffler van der Waals correction method with and without self-consistent screening applied to solids. *Phys Rev B* **87**, 064110 (2013).
55. G Kresse, D Joubert, From ultrasoft pseudopotentials to the projector augmented-wave method. *Phys Rev B* **59**, 1758–1775 (1999).
56. V Blum, et al., *Ab initio* molecular simulations with numeric atom-centered orbitals. *Comput Phys Commun* **180**, 2175–2196 (2009).
57. HJ Monkhorst, JD Pack, Special points for Brillouin-zone integrations. *Phys Rev B* **13**, 5188–5192 (1976).